SUPPLEMENTARY FIGURES AND TABLES

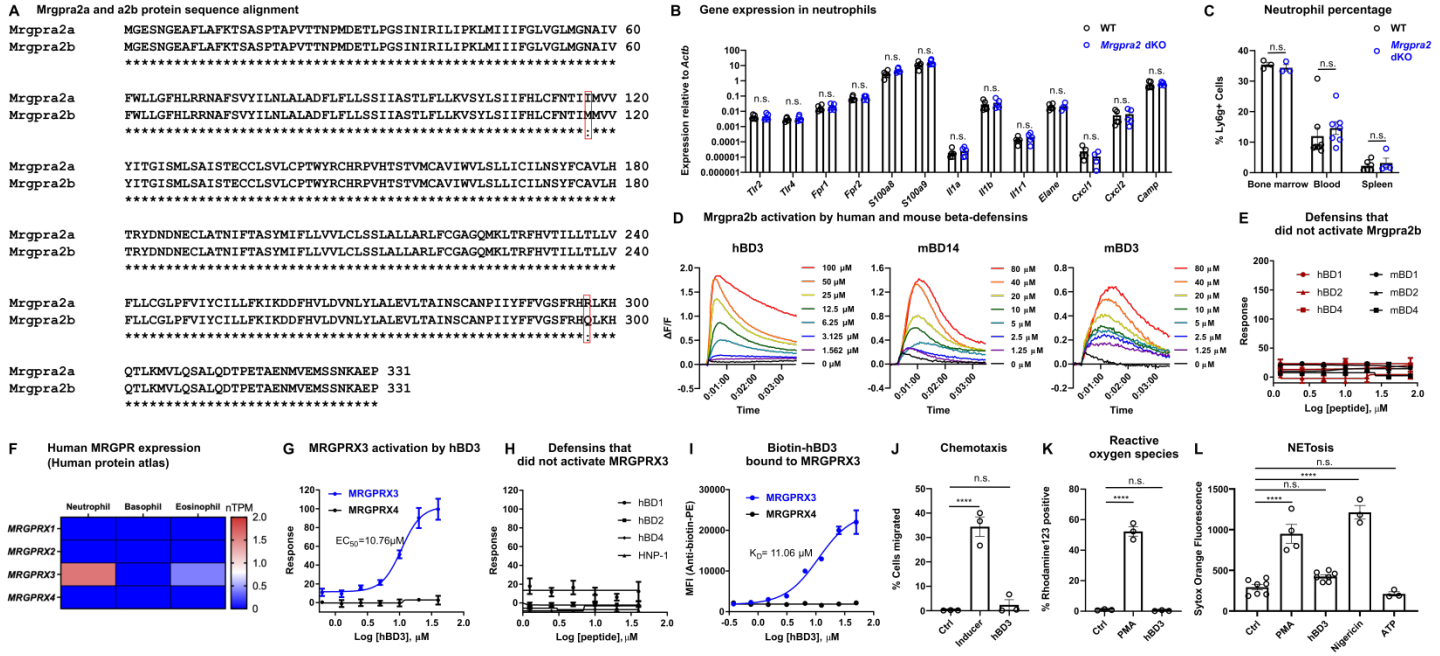

Figure S1. Ligand-receptor interactions between defensins and Mrgpr receptors

(A) Protein sequence alignment between Mrgpra2a and Mrgpra2b by Clustal Omega. The amino acids that differ between the two proteins were highlighted in red boxes.

(B) qPCR quantifications of key genes in neutrophils purified from WT (black) or *Mrgpra2* dKO (blue) mice. The amounts of mRNA transcripts were normalized to housekeeping gene *Actb*. n=5

(C) Percentage of Ly6g+ neutrophils in bone marrow, blood and spleen of WT and *Mrgpra2* dKO animals measured by flow cytometry. n=3-8

(D) Representative FLIPR Ca^{2+} traces showing hBD3, mBD14 and mBD3 activation of Mrgpra2b. Related to Figure 1E.

(E) HEK cells expressing Mrgpra2b were not activated by human peptides hBD1, 2, 4 or mouse peptides mBD1, 2, 4 as determined by FLIPR intracellular calcium mobilization assay. n=2

(F) Heatmap showing the expression of *MRGPRX1-X4* in human neutrophils, basophils and eosinophils based on the Human Protein Atlas.

(G) HEK cells expressing MRGPRX3 activation by hBD3 (EC_{50}=10.76μM) as determined by FLIPR intracellular calcium mobilization assay. Cells expressing MRGPRX4 were not activated and used as negative control. n=5

(H) HEK cells expressing MRGPRX3 were not activated by human beta-defensins hBD1, 2, 4 or human alpha-defensin HNP-1. n=3

(I) Dissociation constant (K_D=11.06μM) between biotin-hBD3 and MRGPRX3 determined by flow cytometry. Cells expressing MRGPRX4 were used as negative control. n=3

(J) hBD3 did not trigger chemotaxis of WT neutrophils, migration inducer (Abcam) was used as positive control. n=3

(K) hBD3 did not trigger production of reactive oxygen species in WT neutrophils. PMA was used as positive control. n=3

(L) hBD3 did not trigger NETosis of purified WT neutrophils. PMA and nigericin were used as positive controls, medium and ATP were used as negative controls. n=3-7

Results are presented as mean ± SEM from at least two independent experiments. ****$p < 0.0001$, n.s. not significant by one-way (H-J) or two-way ANOVA (B-C).

Related to Figure 1

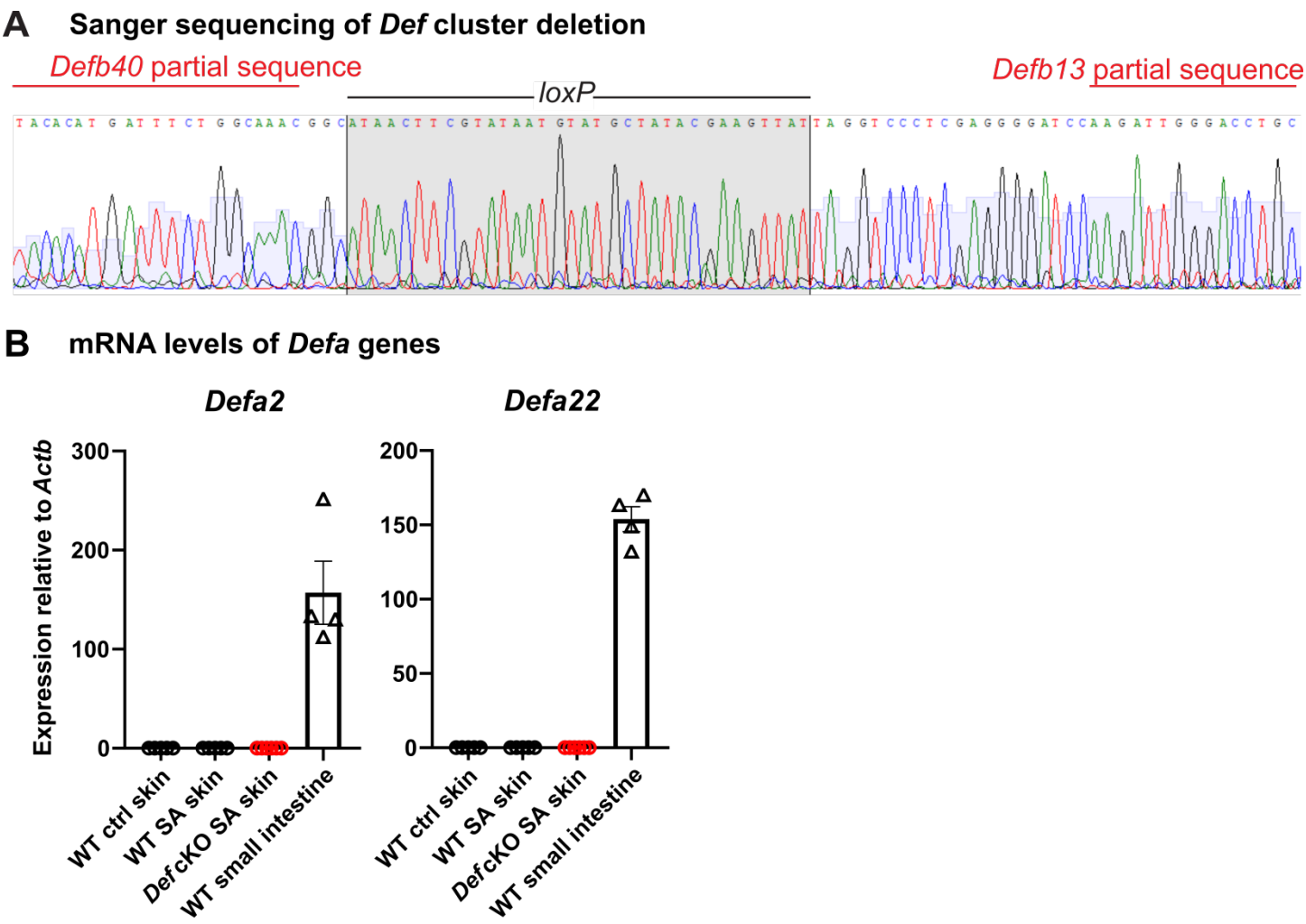

Figure S2. Validations of the *Def* cKO mouse

(A) Sanger sequencing result of *Def* cKO deletion band showing one recombined *loxP* sequence flanked by partial sequences of *Defb40* and *Defb13* genes.

(B) Relative expressions of *Defa2* and *Defa22* in WT control skin, WT skin 24 hours post *S. aureus* infection (black circles), *Def* cKO skin 24 hours post *S. aureus* infection (red circles) and WT small intestine (black triangles). mRNA expressions were normalized to housekeeping gene *Actb*. n=4-6 Results are presented as mean ± SEM from at least two independent experiments.

Related to Figure 2

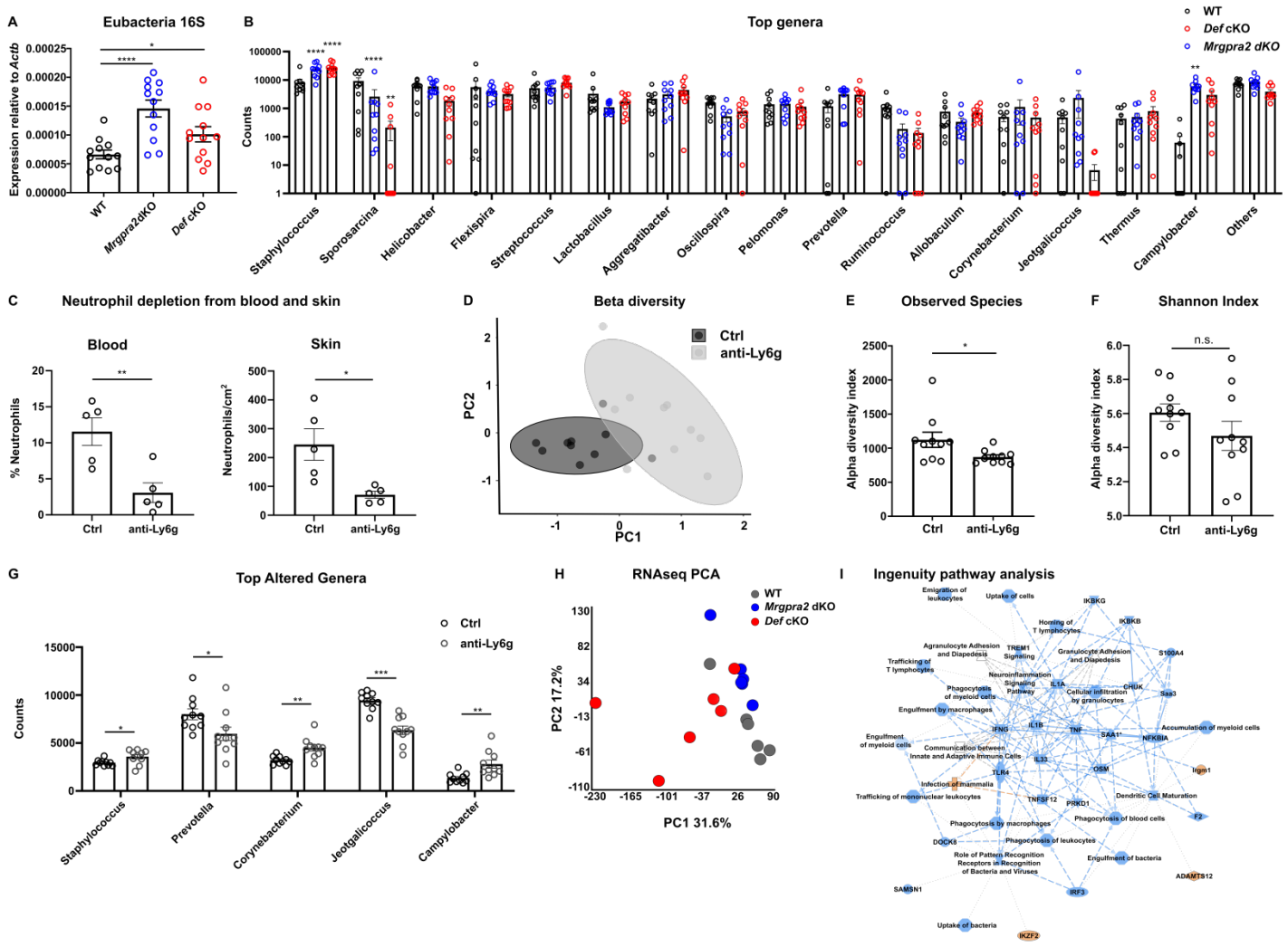

Figure S3. Skin microbiome dysbiosis in *Mrgpra2* dKO, *Def* cKO and neutrophil depleted animals

(A) qPCR of eubacterial 16S rRNA in WT (black), *Mrgpra2* dKO (blue) and *Def* cKO (red) skin. RNA levels were normalized to housekeeping gene *Actb*. n=12

(B) Top genera of WT (black), *Mrgpra2* dKO (blue) and *Def* cKO (red) skin microbiota.

One-way ANOVA were used to compare each mutant strain with WT. Non-significant tests were not labeled.

(C) Percentage of neutrophils in the blood and neutrophils per cm^2 in the skin in mice treated with control or anti-Ly6g antibody. Antibody depletion caused a 70-80% reduction in neutrophils in both blood and naïve skin. n=5

(D-G) 16S sequencing analysis of microbial communities on the skin of WT mice treated with control or anti-Ly6g antibodies for two weeks. n=10

(D) Principal coordinates analysis showing that the clustering of anti-Ly6g treated (light grey) microbial communities distinct from that of control WT (dark grey).

(E) Total numbers of bacterial species observed in control WT (dark grey) and neutrophil-depleted (anti-Ly6g-treated) (light grey) skin swab samples.

(F) Shannon indices of control WT (dark grey) and neutrophil-depleted (anti-Ly6g-treated) (light grey) skin swab samples.

(G) Top altered genera between control WT (dark grey) and neutrophil-depleted (anti-Ly6g-treated) (light grey) skin microbiota.

(H) Principal component analysis (PCA) of RNAseq results revealed differential clustering of WT (grey), *Mrgpra2* dKO (blue) and *Def* cKO (red) gene expressions.

(I) Ingenuity gene ontology pathways analysis of genes affected in both *Mrgpra2* dKO and *Def* cKO naïve skin compared to WT.

Results are presented as mean ± SEM from at least three independent experiments for (A) and from one experiment for (B-I). *p<0.05, **p<0.01, ***p<0.001, ****p < 0.0001, n.s. not significant by one-way ANOVA (A, B, G) or two-tailed unpaired Student's t test (C, E, F).

Related to Figure 3

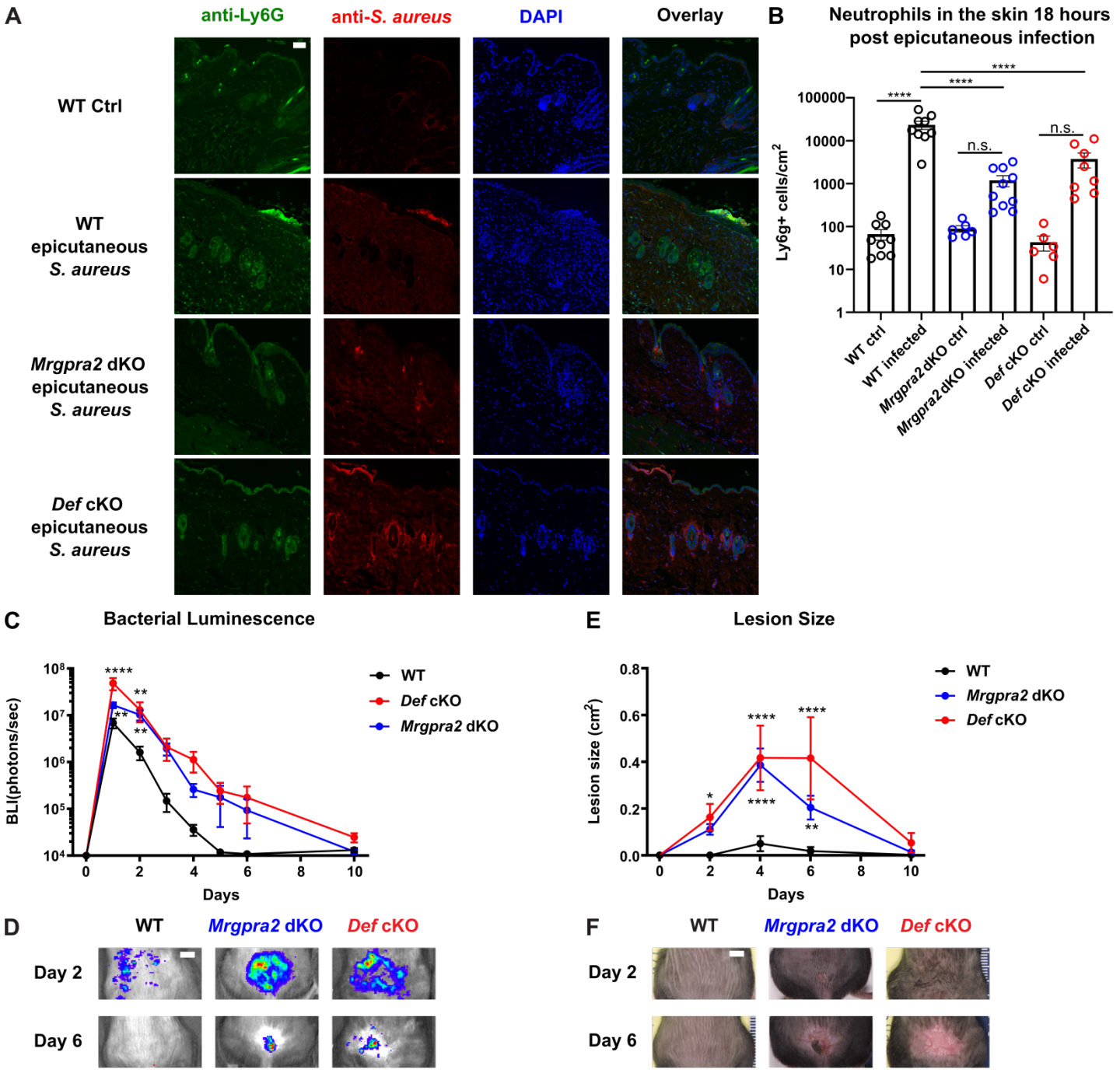

Figure S4. Mrgpra2 and defensins were necessary for clearing epicutaneous *S. aureus*

(A) Immunofluorescent images showing neutrophils stained with anti-Ly6G (green), *S. aureus* (red) and DAPI (blue) in WT ctrl skin (top row), and WT, *Mrgpra2* dKO, and *Def* cKO skin 18 hours post-epicutaneous *S. aureus* application (bottom three rows). A significant number of neutrophils infiltrated into the WT skin and were located close to the dermis or hair follicles where the bacteria colonize (second row, green dots in anti-Ly6G image). *Mrgpra2* dKO and *Def* cKO animals had less neutrophils infiltrating into the skin in response to the epicutaneous *S. aureus* challenge. Scale bar=100μm

(B) Flow cytometry analyses of neutrophils in the skin 18 hours post-epicutaneous *S. aureus* application. Both *Mrgpra2* dKO and *Def* cKO animals showed reduced numbers of neutrophils. n=6-9

(C) Bacterial luminescence (Mean total flux [photons per second]) of WT (black, n=8), *Mrgpra2* dKO (blue, n=12) and *Def* cKO (red, n=6) back skin following epicutaneous *S. aureus* application.

(D) Representative images of in vivo bioluminescence. Scale bar=0.5cm

(E) Mean total lesion size (cm^2) of WT (black), *Mrgpra2* dKO (blue) and *Def* cKO (red) back skin following epicutaneous *S. aureus* application.

(F) Representative photographs of lesions. Scale bar=0.5cm

Results are presented as mean ± SEM from at least three independent experiments. *p < 0.05, **p < 0.01, ****p < 0.0001, n.s. not significant by one-way ANOVA (B) or two-way ANOVA (C, E).

Related to Figure 3

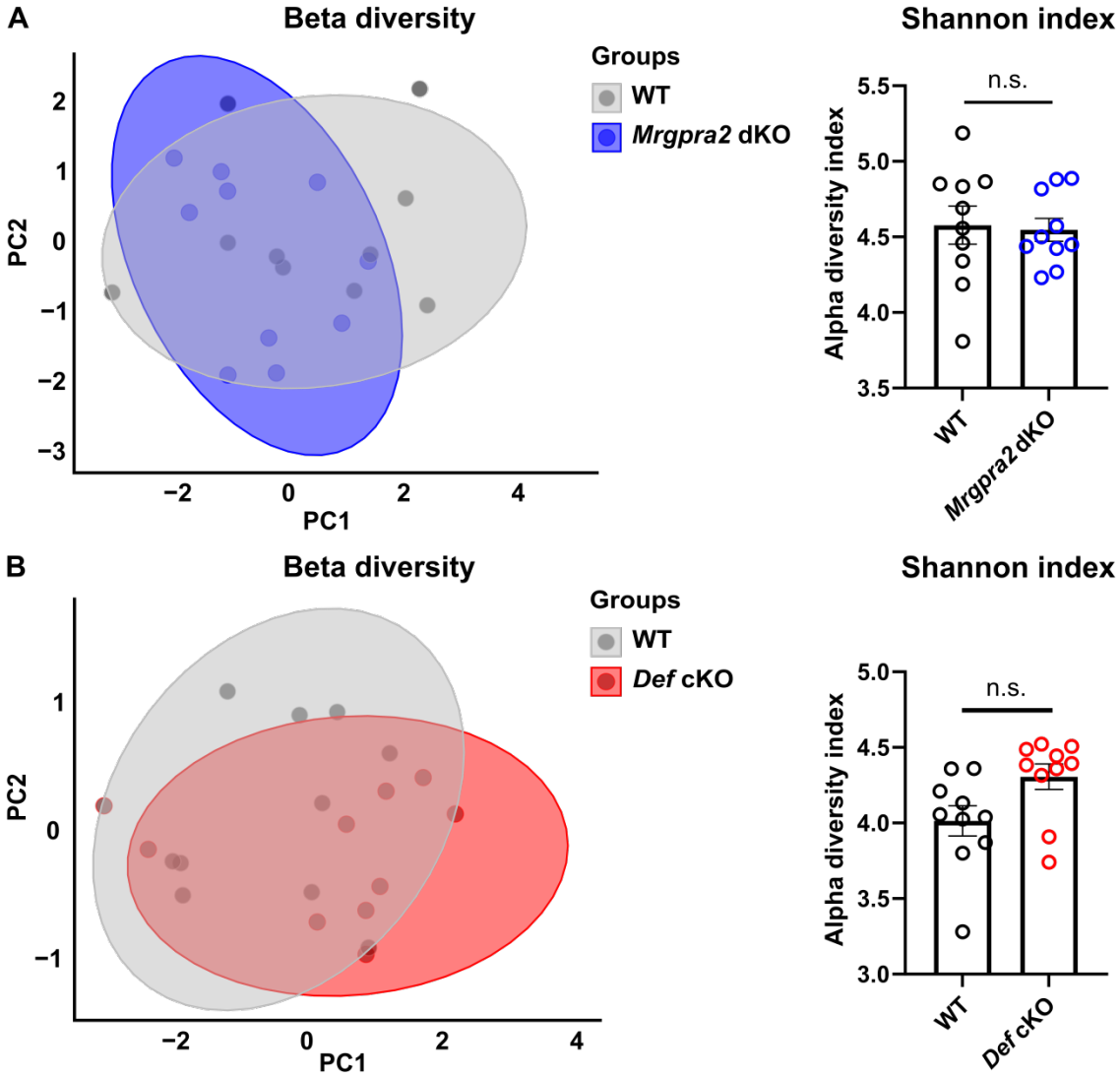
A
Beta diversity
Groups
WT
Mrgpra2 dKO
PC2
PC1
Shannon index
n.s.
Alpha diversity index
WT
Mrgpra2 dKO
B
Beta diversity
Groups
WT
Def cKO
PC2
PC1
Shannon index
n.s.
Alpha diversity index
WT
Def cKO

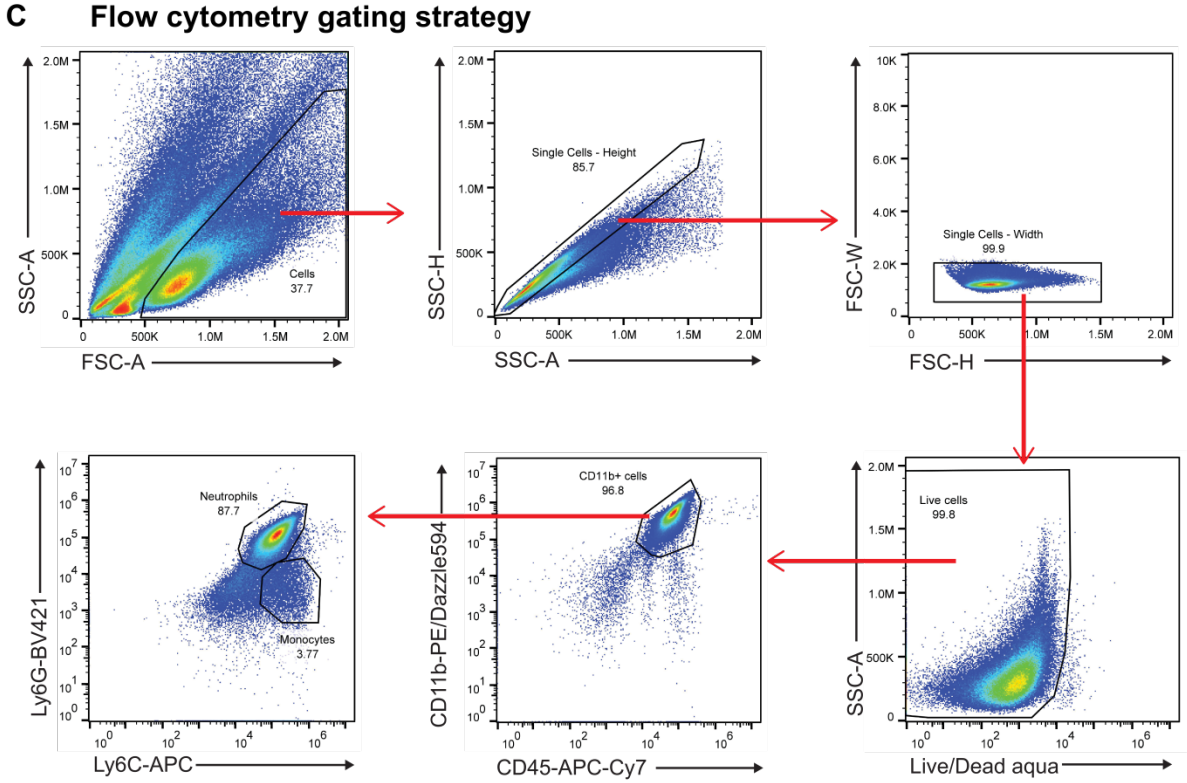
C
Flow cytometry gating strategy
SSC-A
FSC-A
Cells
37.7
SSC-H
SSC-A
Single Cells - Height
85.7
FSC-W
FSC-H
Single Cells - Width
99.9
SSC-A
Live/Dead aqua
Live cells
99.8
CD11b-PE/Dazzle594
CD45-APC-Cy7
CD11b+ cells
96.8
Ly6G-BV421
Ly6C-APC
Neutrophils
87.7
Monocytes
3.77

Figure S5. Analysis of *S. aureus* infected skin

(A-B) 16S sequencing analysis of microbial diversity on the skin of WT animals co-housed with *Mrgpra2* dKO (A) and *Def* cKO (B) mice. Animals housed together share skin microbiomes. Co-housed animals were used for all infection analyses. n=10

(C) Gating strategy for flow cytometry analyses of skin samples.

Results are presented as mean ± SEM from one experiment. n.s. not significant by two-tailed unpaired Student's t test.

Related to Figures 4 and 5

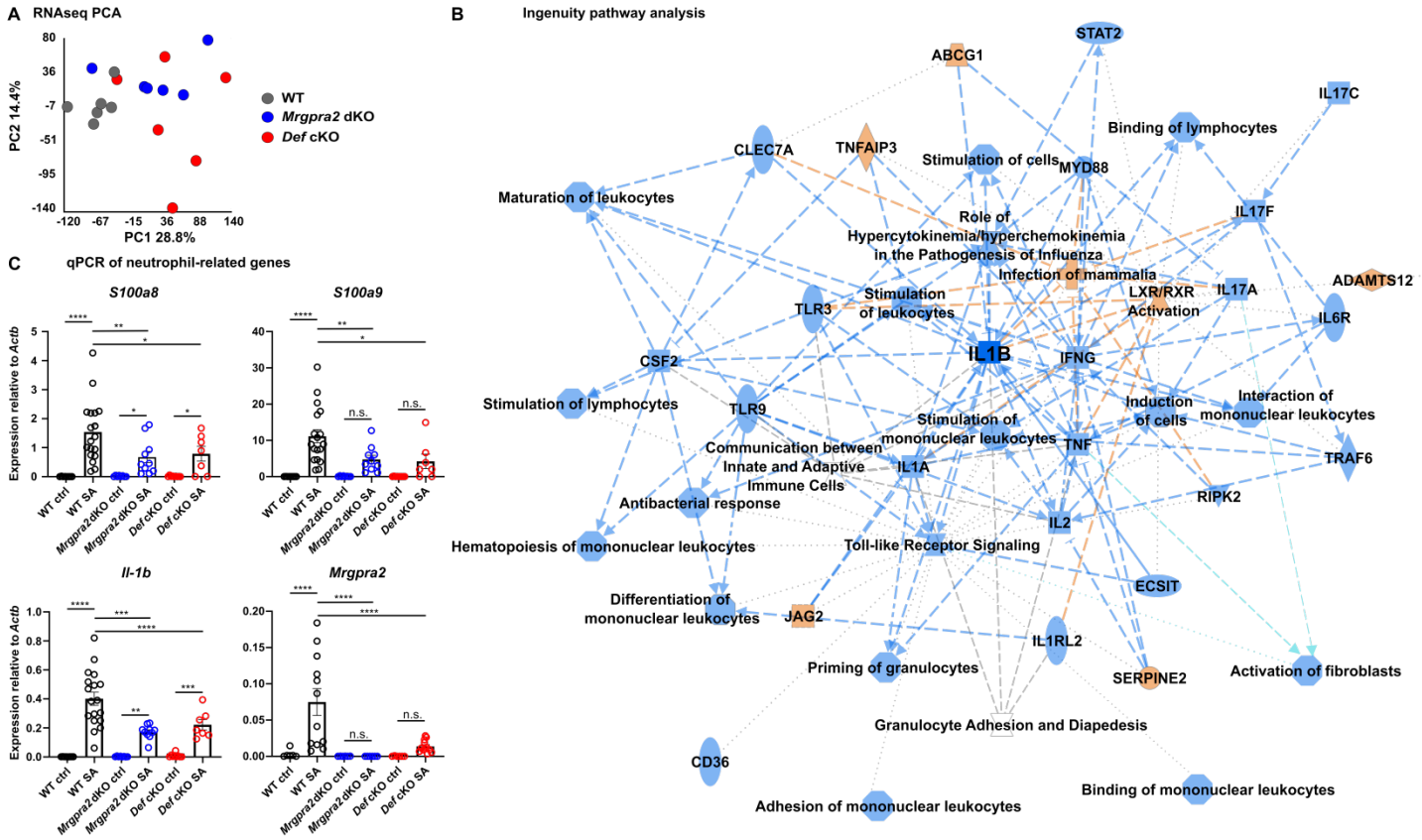

Figure S6. RNAseq analysis of *S. aureus* infected skin

(A) Principal component analysis (PCA) of RNAseq results revealed differential clustering of WT (grey), *Mrgpra2* dKO (blue) and *Def* cKO (red) gene expressions 24 hours post-*S. aureus* infection.

(B) Ingenuity gene ontology pathways analysis revealed a network of genes affected in both *Mrgpra2* dKO and *Def* cKO *S. aureus*-infected skin compared to WT. IL-1β (highlighted in the center) emerged as a main hub in this interconnected network, whose down-regulation potentially drove the defects in antibacterial immunity of the *Mrgpra2* and *Def* mutant animals.

(C) qPCR quantifications of mRNA levels of *S100a8*, *S100a9*, *Il1b* and *Mrgpra2* in the skin of WT, *Def* cKO and *Mrgpra2* dKO mice 24 hours post *S. aureus* infection. n=6-18

Results are presented as mean ± SEM from at least three independent experiments for (C) and from one experiment for (A-B). *p < 0.05, **p < 0.01, ***p < 0.001 ****p < 0.0001, n.s. not significant by two-way ANOVA.

Related to Figure 6

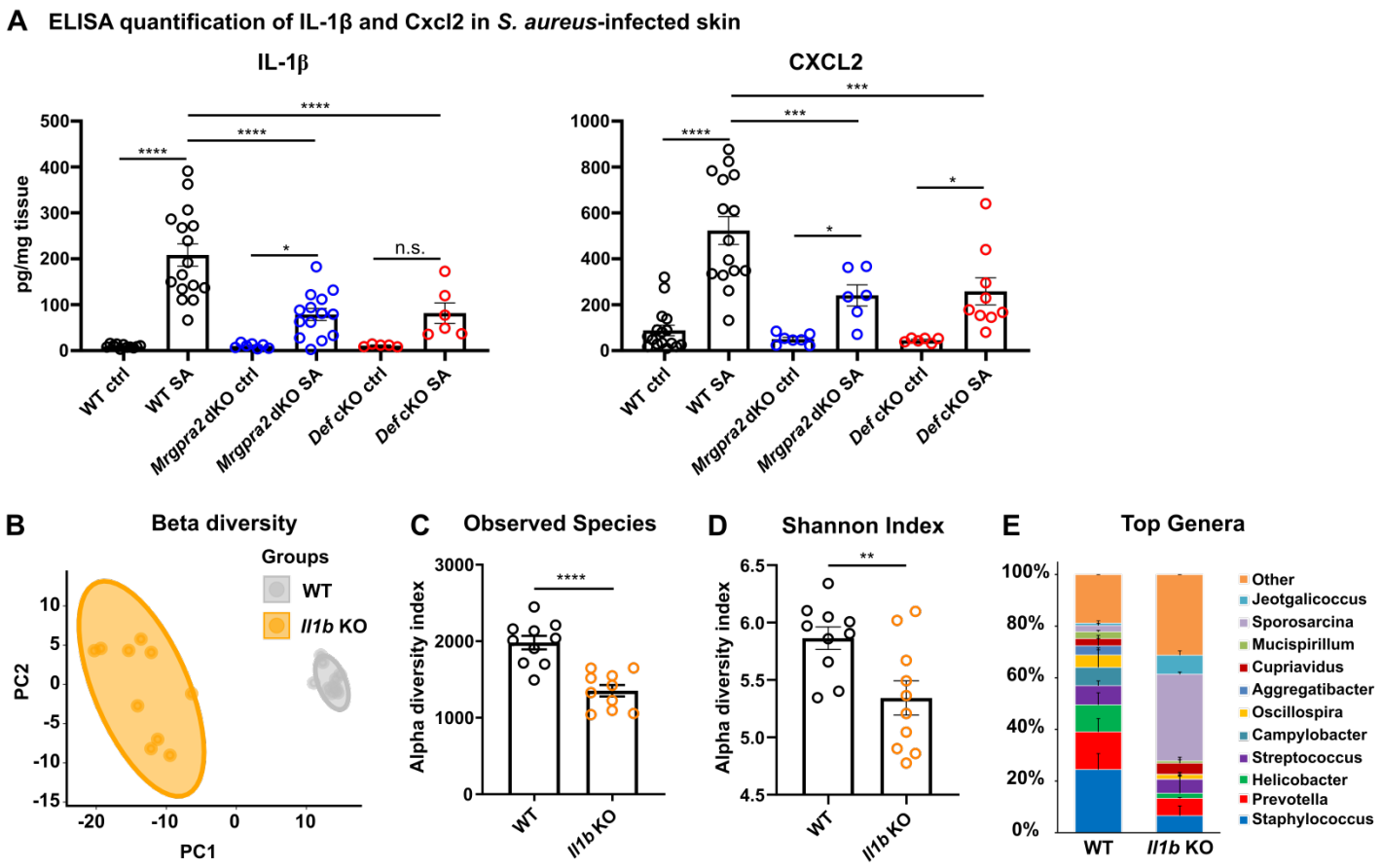

Figure S7. IL-1β and Cxcl2 were downstream of defensin-Mrgpra2 signaling

(A) ELISA quantifications of protein levels of IL-1β and Cxcl2 in the skin of WT, *Def* cKO, and *Mrgpra2* dKO mice 24 hours post *S. aureus* infection. n=5-16

(B-E) Skin dysbiosis in *Il1b* KO animals. n=10

(B) Principal coordinates analysis showing the clustering of *Il1b* KO (yellow) and WT (grey) microbiota.

(C) Total numbers of bacterial species observed in WT (black) and *Il1b* KO (yellow) skin samples.

(D) Shannon indices of WT (black) and *Il1b* KO (yellow) skin swab samples.

(E) Stacked bar charts depicting the relative abundance of top genera in WT and *Il1b* KO skin microbiota.

Results are presented as mean ± SEM from at least three independent experiments for (A) and from one experiment for (B-E). *p<0.05, **p < 0.01, ***p < 0.001, ****p < 0.0001, n.s. not significant by one-way ANOVA in (A) and by two-tailed unpaired Student's t test in (B-D).

Related to Figure 6 and Figure 7

Table S1. Flow cytometry and FACS panels, related to the STAR methods section

Tissue Types	Antigen	Fluorochrome	Company	Catalog #	Clone
Skin		Live/Dead Aqua	Thermo Fisher	L34966	
	CD45	APC-Cy7	Biolegend	103116	30-F11
	CD11b	PE/Dazzle594	Biolegend	101256	M1/70
	CD11c	PE/Cy7	Biolegend	117318	N418
	Ly6C	APC	Biolegend	128016	HK1.4
	Ly6G	BV421	Biolegend	127628	1A8
	F4/80	BV605	Biolegend	123133	BM8
	Siglec F	BB515	BD Bioscience	564514	E50-2440
Peritoneal Lavage					
Mast cells		Sytox Red	Thermo Fisher	S34859	
	c-Kit	BV421	Biolegend	135124	ACK2
	ICAM	FITC	Biolegend	116105	YN/1.7.4
	F4/80	PE	Biolegend	123110	BM8
	FcεRI	PE/Cy7	Biolegend	134318	MAR-1
Macrophages		Sytox Red	Thermo Fisher	S34859	
	Ly6G	BV421	Biolegend	127628	1A8
	ICAM	FITC	Biolegend	116105	YN/1.7.4
	F4/80	PE	Biolegend	123110	BM8
	CD11b	BV785	Biolegend	101243	M1/70
Spleen					
Dendritic cells		Sytox Blue	Thermo Fisher	S34857	
	CD11c	BV605	Biolegend	117334	N418
	B220	APC	eBioscience	17-0452-82	RA3-6B2
	I-A/I-E	BV711	Biolegend	107643	M5/114.15.2
	Ly6G	PE/Cy7	Biolegend	127617	1A8
Peripheral Blood					
Monocytes		Sytox Blue	Thermo Fisher	S34857	
	CD11b	PE	Biolegend	101207	M1/70

	B220	APC	eBioscience	17-0452-82	RA3-6B2
	Ly6G	AF700	Biolegend	127622	1A8
	TCRβ	BV785	Biolegend	109249	H57-597
Eosinophils		Sytox Red	Thermo Fisher	S34859	
	Ly6G	BV421	Biolegend	127628	1A8
	SiglecF	BB515	BD Bioscience	564514	E50-2440
	CD49b	PE	Biolegend	108908	DX5
	CD11b	BV785	Biolegend	101243	M1/70
Bone Marrow					
Neutrophils		Sytox Red	Thermo Fisher	S34859	
	Ly6G	BV421	Biolegend	127628	1A8
	SiglecF	BB515	BD Bioscience	564514	E50-2440
	CD49b	PE	Biolegend	108908	DX5
	CD11b	BV785	Biolegend	101243	M1/70
Basophils		Sytox Red	Thermo Fisher	S34859	
	c-Kit	BV421	Biolegend	135124	ACK2
	SiglecF	BB515	BD Bioscience	564514	E50-2440
	CD49b	PE	Biolegend	108908	DX5
	FcεRI	PE/Cy7	Biolegend	134318	MAR-1